Check for updates

Synthesis and characterization of Au–ZnO nanorods growth by CVD method

Sabah Jameel Mezher[1] · Bahjat B. Kadhim[1] · Mohammed O. Dawood[1]

Abstract

On silicon (100) surface substrates, single-crystal ZnO nanorods (NRs) were produced in a CVD (Chemical vabour deposition) home-made reactor with the help of a catalytic Au-seeds layer. Si substrates were coated with an Au- catalyst layer of 20 nm thickness using direct current sputtering (DC sputtering). Au-catalyst layer plays a pivotal role in synthesizing nanostructures by VLS (Vapour–Liquid–Solid) process. Zinc powder [0.2 g] was used as a source, and silicon (100) of 1.0×1.0 cm^2 area was used as a substrate. We utilized a mixture of argon/oxygen gases (40/10 flow rate) with 700 °C growth temperature for 1 h to ZnO NRs formation. The Au–ZnO NRs were characterized by XRD (X-ray diffraction), AFM (Atomic force microscopy), and FESEM (Field emission scanning electron microscopy) techniques. The results demonstrate that the Au–ZnO NRs are single crystalline and have a hexagonal structure (wurtzite) with a (101) preferred orientation. The sharp and robust diffractions from ZnO NRs confirm that the CVD thermal-grown ZnO NRs have good crystallinity and high purity. The AFM pictures showed that the average particle size of Au–ZnO NRs is 45.31 nm, which is in reasonable agreement with the crystallite sizes estimated from the XRD pattern. The FESEM confirm that the grown ZnO NRs are hexagonal wurtzite NRs. As a whole, Au–ZnO NRs ranged in size from 1.6 to 1.738 μm in length and 250–300 nm in diameter on average. The Au catalyst seed layer acts as a nucleation layer that draws Zn^{2+} and O ions to the substrate's surface and serves as an active site for the growth of ZnO NRs. Those results were accomplished with discussion of the mechanism and model of growth for Au–ZnO NRs.

✉ Sabah Jameel Mezher
   sabah.jamil@uomustansiriyah.edu.iq

   Bahjat B. Kadhim
   sci.phy.bbk@uomustansiriyah.edu.iq

   Mohammed O. Dawood
   mohammedodda2017@uomustansiriyah.edu.iq

1   Department of Physics, College of Science, Mustansiriyah University, Baghdad, Iraq

1 Introduction

The unique properties of nanotechnology have aroused the interest of many researchers due to the entry of this technology into various commercial applications and industries. Nanotechnology's already been adopted by the chemical, mechanical, and technological domains; it's making its way into the medical and drug industries as well (Hana 2019). In recent years, nanotechnology has become an increasingly prevalent area of study across all academic fields. This is because of its many advantageous properties, including its high degree of stability, compact size, large surface area, strong chemical reaction, and low weight (Paul and Robeson 2008). Zinc oxide, one of the most popular nanomaterials, has attracted a lot of attention from researchers and scientists because of its physical and chemical characteristics, including its high stability of photochemical and electrochemical association coefficients, which make it ideal for various industries and medicinal activities (Aysa et al. 2017; Kołodziejczak-Radzimska and Jesionowski 2014; Young and Chu 2021). Zinc oxide is a metal oxide semiconductor that falls into the II–VI group between covalent and ionic semiconductors. There are 1D (one-dimensional), 2D (two-dimensional), and 3D (three-dimensional) structures of zinc oxide, with one-dimensional formations being more common (Kołodziejczak-Radzimska and Jesionowski 2014; Young and Chu 2021; Lockett et al. 2012). The crystalline form of ZnO can take on either the wurtzite (hexagonal symmetry) or rock salt (cubic symmetry) structures, with the former being more common and stable (Saeed 2009).

Zinc oxide is a semiconductor that finds widespread application in many different areas, including electronic displays, electroacoustics, and photocatalysis devices (Chu et al. 2022). Zinc oxide's thermal and chemical stability, piezoelectric and photoelectric properties, and other attributes make it an ideal material for use in high-tech applications. These applications range from LEDs (light-emitting diodes) and optical detectors to biological and chemical sensors and energy-collecting devices like solar cells, electromagnetic devices, nanogenerators, etc. (Hahn 2011; Shi et al. 2021; Yu et al. 2016; Young and Lai 2021). The use of nanostructured zinc oxide was not limited to these fields only; it was an important element in the medical field, where it witnessed a remarkable development in the use of nanotechnology, where nanoparticles can be manufactured in the shape and size specified for the required purpose. In addition to these applications, the medical industry has seen significant progress thanks to nanotechnology, which allows nanoparticles to be made in the form and size required for the needed purpose, making zinc oxide nanomaterials an essential component, as it may lead to novel approaches to treating diseases that, until now, have been hard to zero in on because of size limitations (Wahab et al. 2012; Mirzaei and Darroudi 2017).

Many various chemical and physical techniques, including thermal evaporation (Alsultany and Ghazia 2018; Young et al. 2021), CVD (chemical vapour deposition) (Kim et al. 2019), CBD (chemical bath deposition) (Rosli et al. 2022), PVD (physical vapour deposition) (Kong et al. 2001), SGD (sol–gel deposition) (Alwan et al. 2015), ECP (electrochemical precipitation) (Gupta et al. 2013), and pulsed laser ablation (Navas et al. 2017), can be used to produce the zinc oxide nanostructures.

The CVD technique may be considered the most popular technique for the precipitation of zinc oxide structures on metal-catalyzed substrates using gold as the favourite catalyst (Levitt 1971). However, it has been noted in some recent research that the properties of the VLS mechanism are inconsistent with zinc oxide synthesis that is catalysed by gold (Li et al. 2006; Lim et al. 2006). These investigations indicate that the as-grown nanostructure

is produced by the VS (vapour-solid) growth mechanism. Understanding the mechanism of growth and improv strategies to control the morphology are prerequisites for fabricating ZnO nanostructures with many acceptable morphologies for commercial use. For instance, nanorods with good alignment seem to be the optimal choice for field emitters and UV/ white light emitting devices, and nanorods seem particularly well suited for use as interconnects in nanoelectronic systems and gas sensors (Kumar et al. 2008).

Siegel and co-workers investigated the crystalline structures and optical characteristics of gold nanofilms deposited on glass substrates that were produced using DC sputtering. They proved that gold nanolayers display both metallic and semiconducting-like kind of conductivity. Kumar and co-workers used a CVD reactor to grow single crystalline ZnO NRs on silicon substrates and analyzed their properties. CVD parameters, like temperature, reaction time, and catalyst layer thickness/morphology have been shown to play an important influence in the formation of nanostructures using the VLS mechanism, and by fine-tuning these CVD parameters, highly controlled guided formation of ZnO NRs has been accomplished (Kumar et al. 2018). N. Rusli and co-authors studied ZnO NRs formation at grow temperatures from 600 to 1000 C by the thermally evaporated technique in the presence of oxygen (O_2) gas. It has been shown that the surface roughness of the Si substrates plays a role in the formation of high-density ZnO NRs covering a broad area, where appropriate planes have been provided to promote the precipitate of Zn or ZnO seeds for use as sites of nucleation in the consecutive growth of ZnO NRs. Their research indicates that the initial seed structure significantly affects the growth of ZnO nanostructures and must be taken into account when studying the mechanism in further detail (Rusli et al. 2012).

In this paper, ZnO NRs were synthesized using the VLS process by depositing an Au seed layer catalyst of 20 nm thickness on Si substrates using a home-made furnace by the CVD method. In most of the previous works found in the literature, a layer of annealed catalyst metal was used at a certain temperature. In this work, and for the first time, we managed to form Au nano-islands without any annealing treatment and used them to grow ZnO NRs, which played a major role in determining the diameter of the grown ZnO NRs. We also used various techniques, including XRD, AFM, and FESEM analysis, to investigate and evaluate the crystal structure, shape, and quality of the produced nanostructured nanofilms.

2 Experimental details

To improve the adherence of the catalyst-free ZnO film (or Au seed layer) onto Si substrates, it is necessary to remove surface contamination and establish a cleaner Si surface. In order to become ready, the Si substrate first was cleaned. Following a gentle washing in soap solution and rinsed with distilled water (DI) water, pieces of Si (1.0×1.0 cm^2) substrates were stirred continuously in acetone and isopropyl alcohol for 10 min before being washed again in DI water. At last, they were 5 min drying in a flow of pure nitrogen.

DC sputtering system (3Targate Plasma Sputtering Cotter MTI Corporation) of 1 kV, 4 mA, and 1.5 mbar was used to sputter gold nanoparticles as a catalyst seed layer (20 nm thickness) on some silicon substrates to get approximately 20 nm thick gold film. See Fig. 1.

Zinc powder (Alfa Aesar, 99.9%) was evenly spread in a boat made of alumina that was putted in the middle of the tube quartz. (2.5 cm diameter and 80 cm long) and inserted in a horizontal home-made furnace. Si substrates of 20 nm Au seed layer were
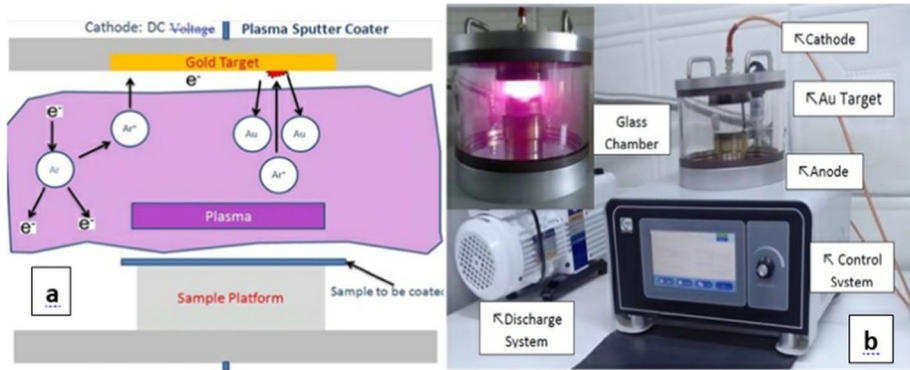
Fig. 1 Show: **a** The plasma process, **b** DC sputtering system

Fig. 2 CVD system ZnO nano-structures growth
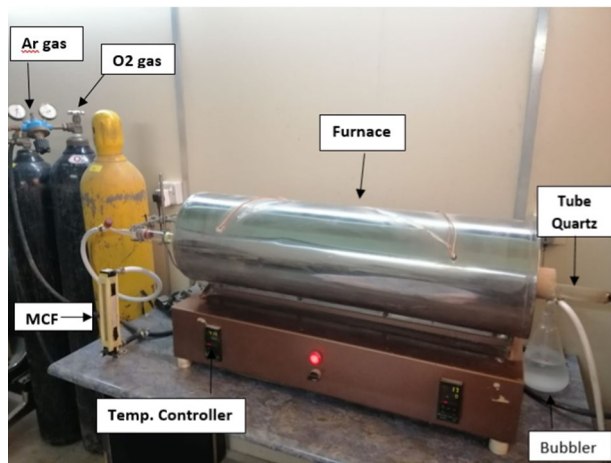
placed at the stove's center. Beginning with the experimental setup, The horizontal tubing was purged with 60 sccm of argon (Ar) gas for just an hour. For purpose of reaching a target temperature (700 °C), this system was heated at a rate of 20 °C/min while maintaining the same volume of argon gas flow. A thermocouple placed in the oven's center allowed for precise temperature control (see Fig. 2). Flowmeters were used to regulate the amount of oxygen and argon gas entering the tube at the pipe inlet. Ar gas flow was lowered to 40 sccm when the target temperature was reached, and O_2 gas was supplied at a rate of 10 sccm at the same time(i.e., 40/10 sccm/min flow rate). It took 1 h to complete the growth experiment. At last, the electricity was turned off, and the furnace was allowed to cool to room temperature, and opening the end of the quartz tube from the bubbler side (ambient atmosphere). A thin layer of grey-white material, identified as ZnO-formed nanostructure, is shown covering the gold–silicon substrates.

An X-ray diffractometer was used to look at the manufactured ZnO nanofilms' structures (X'Pert High Score PANalytical 021-44862778, Philips PW1730) that using CuK_α radiation ($\lambda = 1.54056$ Å) at 40 kV and 30 mA. The samples were studied using FESEM

(scanning electron microscopy JEOL S-5200) and AFM (atomic force microscopy AA2000/SPM). ZnO nanostructures were produced on a substrate, and the effect of the Au seed layer and the growth mechanism on the resulting morphology was studied. Figure 3: Flowchart illustrating the practical stages for preparing the Au–ZnO NRs.

3 Results and discussion

3.1 XRD characterization

By using an X-ray diffractometer, the crystallinity of Au–ZnO films could be determined. Figure 4 shows the XRD patterns of the Au–ZnO nanostructure. The diffraction peaks are all indexed to the diffractions from hexagonal wurtzite ZnO (which concede with JCPDS 36-1451 Card Report). It can be seen that several Au catalyst diffraction peaks are indexed to the diffractions from the FCC gold seed layer (JCPDS 00-004-0784 Card Report). The XRD analysis, in which various planes of reflection predominate, shows that Au is present in the sample. Within an angular inaccuracy of 0.10 of the XRD device, all of the reflection sites match those predicted for native Au. The sharp and robust diffractions from ZnO confirm that the CVD thermal-grown ZnO NRs have good crystallinity with high purity (Singh and Vishwakarma 2015).

Fig. 3 Flowchart illustrating practical stages for preparing and characterizing Au–ZnO NRs
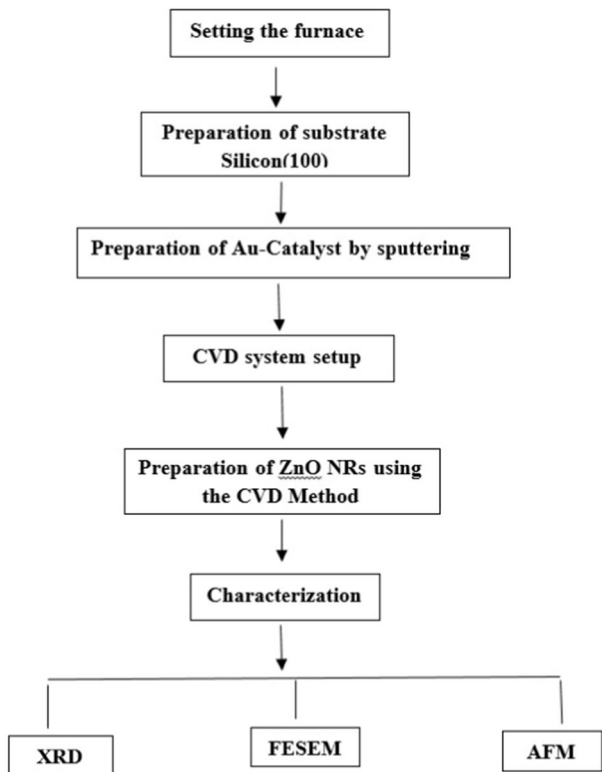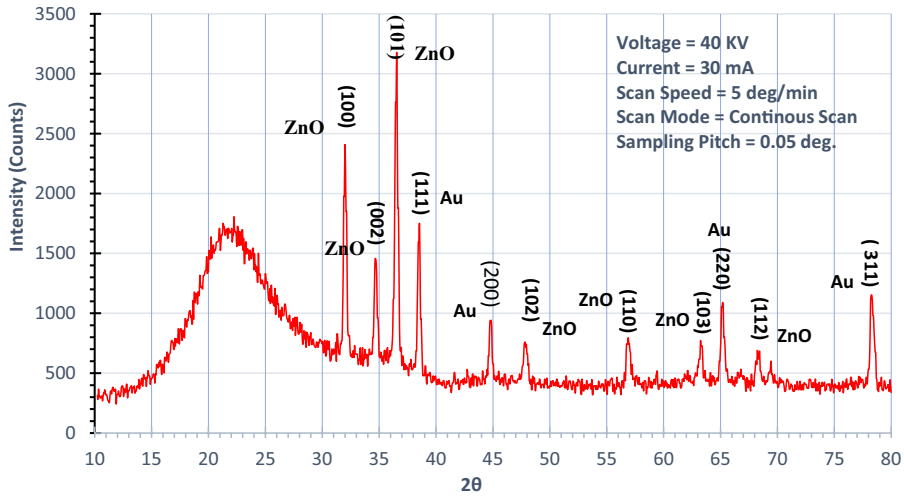
Fig. 4 X-ray diffraction an excellent crystalline structure formation of ZnO NRs

Table 1 displays a comparison between the observed peak height intensities and inter-planar spacing and their average values. Many scientists have researched the hexagonal wurtzite crystal structure, and it turns out that all the peaks in the ZnO output that was obtained are consistent with this structure (Mazhdi and Hossein 2012). Figure 4 shows the discovered peaks at values of 31.9532°, 34.6835°, 36.4893°, 47.8753°, 56.8820°, 63.2627°, and 68.2722° which match the crystal planes (100), (002), (101), (102), (110), (103), and (112) respectively. Some variation in peak intensity and d-spacing between the (100) and (002) crystal lattice planes has been found. Also, the XRD analysis showed no signs of contamination. This demonstrates that highly pure hexagonal ZnO NRs may be produced using this chemical technique, and these results are consistent with those reported in the works of literature (Singh and Vishwakarma 2015; Schulz and Thiemann 1979).

Table 1 X-ray parameters of ZnO NRs

	(hkl)	2θ(deg)	FWHM (deg.)	Crystallite size D(nm)	(ε) Strain×10⁻⁴ (lines²/m⁴)	(δ) Disloca-tion×10¹⁴ (1/m²)	d-Spacing Observed Å
ZnO	(100)	31.9532	0.2460	32.4492	9.0909	9.4970	2.8009
	(002)	34.6835	0.2460	32.4492	8.8072	9.4970	2.5864
	(101)	36.4893	0.2952	27.041	10.3301	13.6756	2.4624
	(102)	47.8753	0.3936	20.2810	11.4640	24.3118	1.9000
	(110)	56.8820	0.2952	27.0411	6.9818	13.6756	1.6187
	(103)	63.2627	0.2952	27.0411	5.7289	13.6756	1.4699
	(112)	68.2722	0.3936	20.2810	6.2590	24.3118	1.3738
Au	(111)	38.4905	0.2460	32.4492	8.3781	9.4970	2.3389
	(200)	44.7994	0.2460	32.4492	7.5857	9.4970	2.0231
	(220)	65.1504	0.2952	27.0411	5.3438	13.6756	1.4318
	(311)	78.2412	0.2952	27.0411	2.5355	13.6756	1.2218

Table 1 contains an evaluation of the interplanar spacing (d) based on relation (1), as described by Mazhdi and Hossein (2012), Dinesh et al. (2014),

$$d = \frac{\lambda}{2\,sin\theta} \qquad (1)$$

Lattice constants a and c are described as follows:

$$a = \frac{\lambda}{\sqrt{3}\,sinn\theta} \qquad (2)$$

By employing Eq. (2) described by Cullity et al. (2001), the lattice constant a for the (100) plane was determined to be a = 3.2336 Å, whilst:

$$c = \frac{\lambda}{sin\theta} \qquad (3)$$

whereas for the (002) plane, the constant lattice c was calculated using Eq. (3) as explained by Cullity et al. (2001) and the value was calculated to be c = 5.1687 °C, and consequently, c/a equals 1.5984. In addition, the X-ray diffraction peaks observed for the planes (100), (002), (101), (102), (110), (103), and (112) agree with the (JCPDS 00-036-1451) findings of ZnO. There is a quite close between the experimental d-values and the calculated ones (JCPDS 00-036-1451), which indicate a hexagonal crystal structure. Table 1 summarizes the results of an XRD analysis of the interplanar spacing (d) determined by the respective (h, k, l) planes.

Using the data obtained from XRD patterns, the crystallite size (D) has been determined using the Debye–Scherrer method (Patterson 1939). Relation (4) describes the procedure, and Table 1 displays the obtained values:

$$D = \frac{k\lambda}{\beta\,cos\theta} \qquad (4)$$

Specifically: D = crystallite size (in nm), k constant (= 0.9), λ = wavelength (0.15406 nm), θ = Bragg angle, and β = full width at half maximum (FWHM in radian). There was excellent crystallized formation as indicated by the narrowing of the diffraction peaks with increasing intensity. Additionally, as was previously observed, the nano-sizes of the produced ZnO nanoparticles (Table 1) are reflected in the broadening of the (101) diffract peaks in the Fig. 4. Thus, it is evident that the crystallinity of nanoparticles has improved (Ismail et al. 2018).

In Fig. 4, the broadening of the XRD patterns is observed, which can be attributable to the nanocrystalline nature of the samples and thus reveals that the size of the particles is on the nanoscale (Mazhdi and Hossein 2012). The precipitated Au–ZnO NRs have a large surface area relative to their volume with a reduction in particle size, which implies an increase in surface-specific sites of activity for chemical reaction and photoabsorption. The increased surface area has a dynamic effect on chemical reactions. The energy band gap between the conduction band electrons and the valence band holes increases due to size quantization, which changes the optical characteristics (Mazhdi and Hossein 2012; Kumbhakar et al. 2008). Because of this, ZnO NRs made in this way under the same conditions and parameters are excellent luminous materials for application in UV/VIS lasers, displays, solar cell components, varistors, and gas sensors (Kumbhakar et al. 2008; Cruz-Vázquez et al. 2005).

**Table 2** RMS, S_a, S_y, Particle Size, and Diameter of Au–ZnO films prepared by the CVD method

RMS roughness S_q (nm)	Average roughness S_a (nm)	Average peak to peak Sy nm	Average particle size (nm)	Average diameter (nm)
3.39	2.69	20.2	45.31	39.44

3.2 AFM characteristics

The AFM gives us good information about the surface topography and the surface crystal structure of the precipitated nanofilms. It has long been understood that the optical and electrical properties of transparent conducting oxide films are affected by their surfaces, which are essential parameters in the use of optoelectronic systems applications. Generally, surface film roughness' increasing affects the optical properties of the films; therefore, it is essential to investigate the surface topography of the films (Daniel et al. 2010).

By using the AFM technique, Fig. 5 shows the topography of the Au–ZnO nanostructure prepared by CVD method. This picture clearly depicted nanostructure films with average particle size that could be measured. The average particle size is 45.31 nm. The average particle size obtained from AFM pictures is in reasonable agreement with the crystallite sizes estimated from the XRD pattern for Au–ZnO NRs film shown in Fig. 4, and a rundown of the findings may be found in Table 2.

Figure 5a shows the topographical analytical image of the surface roughness in two dimensions (2D). It was found that the average surface roughness (S_a) was 2.69 nm, indicating reasonable crystalline regularity and good homogeneity. The mean square root value
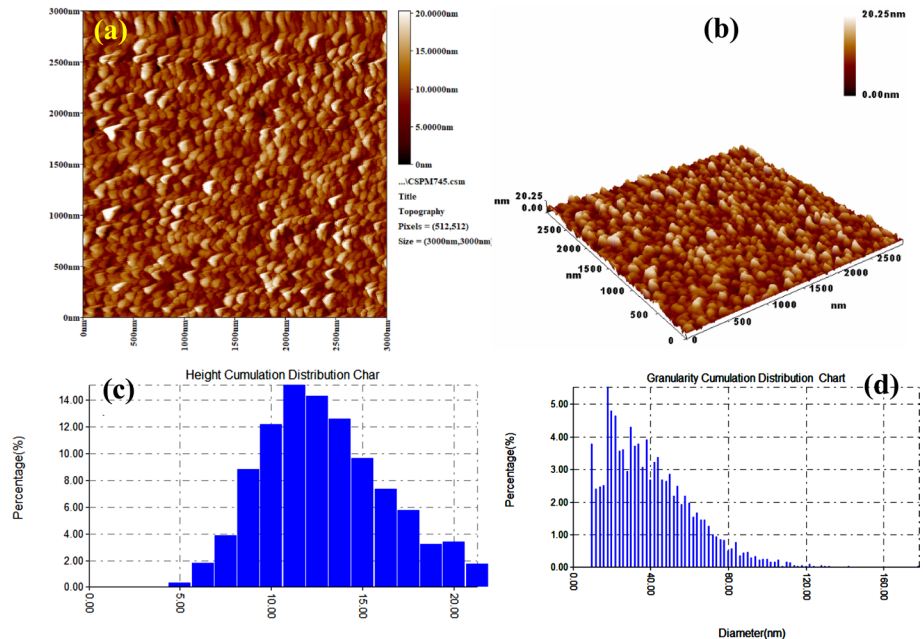
Fig. 5 AFM images of Au–ZnO NRs synthesized by CVD method

(S_q) equals 3.39 nm, showing the surface's smoothness. The higher the mean square root value, the higher the surface roughness, and vice versa (Gadelmawla et al. 2002).

The value of the skewness of the surface plane of the film (S_{sk}) is equal to 0.314. This value shows the surface plane relative to the surface substrate on which the film is deposited, and the maximum value of kurtosis of the surface (S_{ku}) was equal to 3.06 nm; this value shows the topographical appearance of the surface for the film as a whole, and that the average distance between a granule crystalline top to another (S_y peak-peak) equal to 20.2 nm, which indicates the regularity of the deposited film and the possibility of using it in solar cells, because the more uniform the film, the better the reflection (Bhushan 2000). Figure 5b shows a three-dimensional (3D) AFM microscope image of the Au–ZnO film, where we note the regularity in the formation of the film and that the granules are perpendicular to the crystalline axis and are almost equal.

Figure 5c, d shows the AFM microscopic graph of the cumulative distribution of granules grown on the film's surface. It was found that the average granular size was about 39.44 nm, where 10% of the granules had a granulated size of 14 nm and 90% had a coarse size of 68 nm. At the same time, Fig. 3d shows the AFM microscopic graph of the cumulative height distribution of granules which revealed that it is average equal to 12.290 nm, where 10% of the granules had a granular size of 7.5 nm and 90% had a coarse size of 16.25 nm. According to these figures, the observed features of the surface have a grain size of less than 10% of the wavelength of the visible spectrum, which accounts for great optical quality. The large density of ZnO NRs growth which covers a large area may be attributed to the surface roughness that provides ideal planes for promoting the precipitation of Zn, ZnO, or Au catalyst seeds, which serve as the nucleation sites for the consecutive growth of ZnO NRs, and these results are compatible with the research work (Purica et al. 2002).

3.3 FESEM morphological examination

We can see the FESEM photo for ZnO NRs at high magnification in Fig. 6. ZnO NRs were grown using a homemade flow-type reactor performing an elemental VLS phase synthesis process, in which a DC sputtering technique was used to create a seed layer of Au catalyst at 20 nm thickness on a Si (100) substrate. ZnO NRs have indeed formed, as shown in these images. As is apparent from the Fig. 6b, c, the grown ZnO NRs are hexagonal wurtzite nanorods having an average diameter of (250–300) nm and a length of approximately (1.6–1.738) μm with smooth surfaces (see Table 3). Figure 6 shows that the Au catalyst seed layer performs a pivotal role in commanding the diameter of the nanorods by acting as a nucleation layer that draws Zn^{2+} and O ions to the substrate's surface and serves as an active site for the growth of ZnO NRs. In addition, it's important to note that according to the zinc/oxygen partial pressure relationship, catalyst droplet diameter can either decrease or start rising (Zak et al. 2011).

The shape control and morphology of the 1D ZnO nanostructure can be explicated via two mechanisms: the constitution of the catalyst and the conditions of thermodynamics. At a certain temperature, the catalyst is effective for nanostructure forming and based on its certain melting point. The formation of liquid drops and supersaturation may be critical factors for the control of nanostructure morphology and interpret the shapes that are acquired. The mechanism that leads to the forming of one-dimensional ZnO structures depends on phenomena of diffusion, nucleation, and crystallize (Hughes and Wang 2004; Kar et al. 2006), and these results are consistent with the literature (Tseng et al. 2003).

3.4 Growth mechanism

In order to make the most of ZnO NRs in their future uses, it is important to synthesize them in a controlled manner that allows for their desired morphology (Ismail et al. 2018); the mechanism for the formation of ZnO rods is proposed by schematic depicted in Fig. 7. ZnO NRs can be grown on a Si(100) substrate with the help of Au as a catalyst, following these steps: When an Au-coated silicon substrate is heated to 700 °C, a uniform Au layer film undergoes a phase transition from the solid to liquid state, giving rise to monodispersed Au nanoclusters (droplets) with a hemispherical shape. Extended exposure of zinc powder to heat in the atmosphere of a mixture of oxygen and argon leads to the evaporation of zinc and its reaction with oxygen to form zinc oxide vapor, these vapors may provide enough precursors to condense below the molten Au nanoclusters (droplets). After reaching a super-saturation condition, the vapours spread into the Au drops metallic, and the gradient of concentrations in Au clusters leads to ZnO nucleation on a silicon substrate surface in a non-homogeneous (at the interface of the Au cluster and Si substrate) manner. From the Au seed's hemisphere's tip, ZnO is precipitate on a solid silicon substrate to forms nanorods crowned with Au seed; As depicted in the schematic diagram, Au droplets are dislodged off the Si substrate and ride atop the forming ZnO NRs. Droplets of Au catalyst are a favored sink for incoming Zn and O atoms. As time passes, the ZnO NRs lengthen by the aforementioned mechanisms, and this continues unless the growth parameters are altered. As the growth reaction time increases, the size of the ZnO rods will also increase, and they will bend downward consequent to the Au nanoparticles' weight at their tips, and because of this, they get up tangled up with one another. Due to a lattice mismatch between the silicon and zinc oxide, the nano rods that formed are not exactly vertical to the Si substrate surface (Soleimanpour et al. 2012).

The catalysts play a key role in the VLS mechanism of the ZnO nanostructures growth, where it works as nucleation positions and control the diameters growth of ZnO nanostructures (Yi et al. 2005; Huang et al. 2022; Ali et al. 2021; Song and Lim 2007). For 1D ZnO nanostructure growth, Au catalyst may be active at a certain temperature, (at 500 °C and 600 °C), which confirms the role of temperature in super saturation and nanostructure growth of 1D ZnO (Chou and Hsu 2016). The shape control and morphology of the 1D ZnO nanostructure are explicated via two mechanisms: the constitution of the catalyst and the conditions of thermodynamics. At a certain temperature, every catalyst is effective for
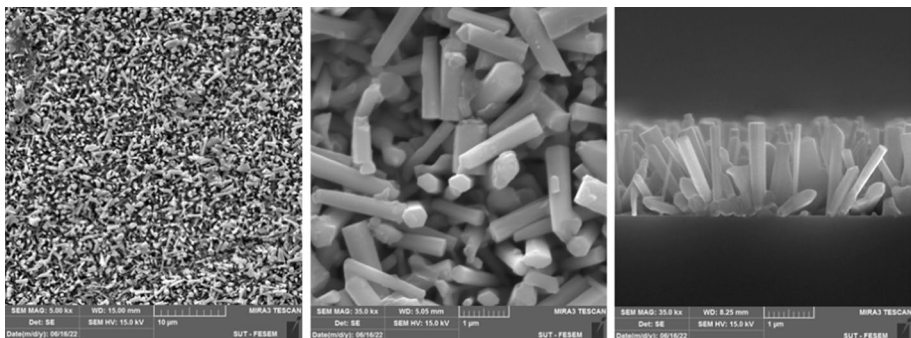

Fig. 6 FESEM of Au–ZnO NRs synthesized by VLS process

Table 3 ZnO NRs with 20 nm Au-catalyst

	Rate of Ar/O sccm	Temperature °C	Average diameter (nm)	Average length (nm)
20 nm Au catalyst	40/10	700	250–300	1.6–1.738

nanostructure forming and based on its certain melting point. The formation of liquid drops and super saturation may be critical factors for the control of nanostructure morphology and interpret the diverse shapes that are acquired. The mechanism that leads to the forming of one-dimensional ZnO structures depends on phenomena of diffusion, nucleation, and crystallize. The temperature plays an important role in the ZnO nanostructure formation by the VLS mechanism (Sangpour et al. 2009; Kaiser et al. 2020). Firstly, ZnO vapor atoms are adsorbed on the surface substrate. The energy of ZnO vapor atoms may be increased by heating the surface substrates from 350 to 600 °C for a quarter-hour, and therefore the diffusion of atoms through the Si surface will be enhanced. At high-temperature processing, the particles of the Au catalyst will aggregate to form liquid clusters to enhance the ZnO vapor condensation. ZnO vapor particles will reach the surface of the Au catalyst droplets and are merged like adatoms. Adatoms are diffused in the clusters, and when the state of super saturation occurs, the segregation may begin to form 1D ZnO nanostructures (Hejazi and Hosseini 2007).

Figure 6 shows Au used as a catalyst to grow ZnO nanostructures. At growth temperatures and by using an Au catalyst, nanorods of ZnO were achieved with good density and aspect ratio (diameter 250–300 nm and a length of approximately 1.6–1.738 μm). Furthermore, ZnO NRs formation is promoted by raising the temperature to 700 °C, which may be interpreted through the ZnO vapour's high prevalence, which affects the ZnO super saturation and leads to ZnO NRs formation with good quality (Kumar et al. 2018). The size of the catalyst NPS controls the NRs diameters for the crystallized ZnO (Wang et al. 2008). The Au catalyst seed layer plays a crucial role in commanding the nanorods diameter by acting as a nucleation layer that draws Zn^{2+} and O ions to the substrates surface and serves as an active site for the growth of ZnO NRs (Sun et al. 2016).

Fig. 7 Growth mechanism of Au catalyst ZnO NRs (Chen et al. 2009)
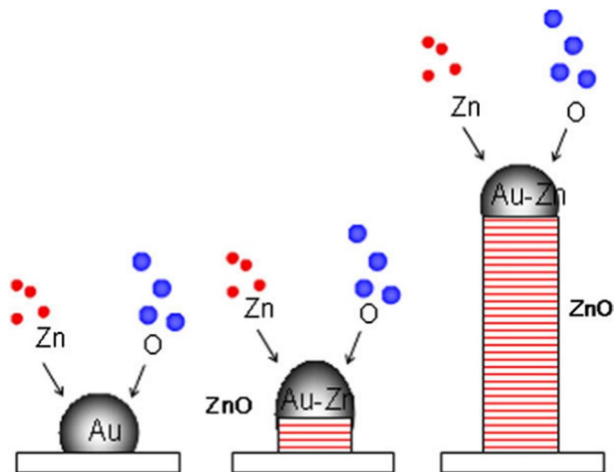
Theoretically, material A is precipitated on substrate surface B when the $\gamma B > \gamma A + \gamma^*$ condition is fulfilled, in which γA the precipitated material surface energy, γB substrate material surface energy, and γ^* interfacial energy. The previous condition not be achieved for Zn precipitate on the Si surface because the Si substrate is usually covered with a thin layer of SiO_2. Zn vapor may be precipitated on Au film in facilely, where Au is stable and possess surface energy higher than Zn (Faisal 2016).

In both the VLS process, the catalyst initiates and directs the growth, and this is why metal nanoparticles are used as catalysts. Growing NRs in a structured and aligned configuration based on the VLS mode requires an epitaxial interaction between the substrate and the NRs. The VLS growth process, which is defined by the presence of a metal particle at the NRs tip, allows for the possibility of diameter and arrangement control via the patterned arrays of catalyst. ZnO has the wurtzite crystal structure with six-fold symmetry in the basal plane. Gold has the face-centred cubic (FCC) structure, the Au [111] planes have three-fold hexagonal-like symmetry, so a Au [111] orientation is also predicted. Therefore, it is expected that ZnO will take the same c-plane crystal orientation as the Au catalyst (Wang et al. 2008).

Few publications have been published on the favorite growth orientation of VLS nanorods. The systematic c-orientation observed in the most recent study likely originates from the VLS process. Since the growth begins at the interface of the liquid–solid, we can anticipate significantly different growth kinetics. As a matter of fact, it has been demonstrated again that Au acts as a catalyst for the ZnO NRs growth. Recent theoretical research has shown that the presence of an Au ad-layer significantly increases the binding energy of a Zn ad-atom on a (000 ± 1) surface. This research also demonstrates that the Zn binding energy on Au–ZnO $(000\bar{1})$ (O-terminated) is 0.38 eV higher than on Au–ZnO (0001) (Zn-terminated). The LDOS (local density of states) indicates the $(000\bar{1})$ polar face's specific chemical activity. Accordingly, it may be more energetically favorable for VLS NRs with c-orientation to grow if Zn atoms migrating from the liquid Au droplet are caught at the Au–ZnO $(000\bar{1})$ (O-terminated) polar face (Faisal et al. 2020; Han 2010).

At growth temperatures and by using Au catalyst, nanoros of ZnO will achieved with high density and a large aspect ratio. Furthermore, ZnO NRs forming is promoted by raising the temperature, which may be interpreted through the ZnO vapour's high prevalence that affects the ZnO super saturation and leads to the ZnO NRs formation with good quality. The size of the catalyst NPs controls the NRs diameters for the crystallized ZnO (Wang et al. 2008).

4 Conclusion

In conclusion, We have used the VLS growth technique using Au as a catalyst to create ZnO NRs on a Si (100) substrate. The procedure results in ZnO NRs grown on a Si substrate in a nearly crosslinked orientation. By using the CVD method, high-purity hexagonal ZnO NRs could be obtain. The XRD test reveals peaks become narrow at higher densities, which indicates the construction of a good crystal structure. The analysis of ZnO NRs by FESEM and AFM shows that they grow epitaxially as hexagonal poles in the [0001] direction. According to our observations, four crucial facts emerged: (1) The nucleation and development of nanorods requires molten metal droplets, which can be obtained by coating the top surface with a metal layer of the appropriate thickness, (2) ZnO NRs have a gold seed at their tip, and the seed is a hemisphere, (3) For optimal nanorod growth, the furnace

must be set at a specific temperature, and (4) As the reaction and growth period increase, the length of the nanorods also increases.

Declarations

Conflict of interest The authors declare no competing interests.

Consent to participate Not applicable.

Consent for publication Not applicable.

Ethics approval Not applicable.

References

Ali, M.N., Salman, S.A., Dawood, M.O.: The growth mechanism of ZnO nanorods and the effects of growth conditions. NVEO-NAT. VOLATILES Essent. OILS J. NVEO **8**(6), 1611–1620 (2021)

Alsultany, F.H., Ghazia, R.A.: Seed/catalyst-free growth of 2D and 3D ZnO nanostructures on glass substrate by thermal evaporation method: effects of carrier gas flow rate. Al-Mustansiriyah J. Sci. **29**(3), 129–132 (2018)

Alwan, R.M., et al.: Synthesis of zinc oxide nanoparticles via sol–gel route and their characterization. Nanosci. Nanotechnol. **5**(1), 1–6 (2015)

Aysa, N.H., Al-Maamori, M.H., Al-Maamori, N.A.A.: Preparation and surface modification of zinc oxide nanoparticles. J. Babylon Univ. Appl. Sci. **25**, 497–503 (2017)

Bhushan, B.: Surface roughness analysis and measurement techniques. In: Modern Tribology Handbook, Two Volume Set, pp. 79–150. CRC Press (2000)

Chen, J.-Y., Pan, C.-J., Tsao, F.-C., Kuo, C.-H., Chi, G.-C., Pong, B.-J., ... & Pearton, S.-J.: Characterization of ZnO nanowires grown on Si (100) with and without Au catalyst. Vacuum, **83**(7), 1076–1079 (2009) https://doi.org/10.1016/j.vacuum.2009.02.001

Chou, H.-T., Hsu, H.-C.: The effect of annealing temperatures to prepare ZnO seeds layer on ZnO nanorods array/TiO2 nanoparticles photoanode. Solid-State Electron. **116**, 15–21 (2016)

Chu, Y.-L., Liu, Y.-H., Chu, T.-T., Young, S.-J.: Improved UV-sensing of Au-decorated ZnO nanostructure MSM photodetectors. IEEE Sens. J. **22**(6), 5644–5650 (2022)

Cruz-Vázquez, C., Bernal, R., Burruel-Ibarra, S.E., Grijalva-Monteverde, H., Barboza-Flores, M.: Thermoluminescence properties of new ZnO nanophosphors exposed to beta irradiation. Opt. Mater. (amst) **27**(7), 1235–1239 (2005)

Cullity, B.D., Stock, S.R.: Elements of X-Ray Diffraction, p. 388. Prentice Hall, Up Saddle River, NJ (2001)

Daniel, G.P., Justinvictor, V.B., Nair, P.B., Joy, K., Koshy, P., Thomas, P.V.: Effect of annealing temperature on the structural and optical properties of ZnO thin films prepared by RF magnetron sputtering. Phys. B Condens. Matter **405**(7), 1782–1786 (2010)

Dinesh, V.P., et al.: Plasmon-mediated, highly enhanced photocatalytic degradation of industrial textile dyes using hybrid ZnO@ Ag core–shell nanorods. RSC Adv. **4**(103), 58930–58940 (2014)

Faisal, A.D.: Optimization of CVD parameters for long ZnO NWs grown on ITO/glass substrate. Bull. Mater. Sci. **39**, 1635–1643 (2016)

Faisal, A.D., Dawood, M.O., Hussein, H.H., Hassoon, K.I.: Performance of ph sensor electrode based on ZnO NRs on Fto-glass substrate. Surf. Rev. Lett. **27**(08), 1950198 (2020)

Gadelmawla, E.S., Koura, M.M., Maksoud, T.M.A., Elewa, I.M., Soliman, H.H.: Roughness parameters. J. Mater. Process. Technol. **123**(1), 133–145 (2002)

Gupta, A.K., Kashyap, V., Gupta, B.K., Nandi, S.P., Saxena, K., Khare, N.: Synthesis of ZnO nanorods by electrochemical deposition method and its antibacterial activity. J. Nanoeng. Nanomanufacturing **3**(4), 348–352 (2013)

Hahn, Y.-B.: Zinc oxide nanostructures and their applications. Korean J. Chem. Eng. **28**, 1797–1813 (2011)

Han, S. K., et al.: Growth and optical properties of ZnO nanorods prepared through hydrothermal growth followed by chemical vapor deposition. In: 2010 3rd International Nanoelectronics Conference (INEC), pp. 1098–1099. IEEE (2010)

Hana, H.E.S.P.D.: Adsorption Study of the Interaction Between Zinc Oxide Nanoparticles with Albumin and Creatinine. University of Kerbala, Karbala (2019)

Hejazi, S.R., Hosseini, H.R.M.: A diffusion-controlled kinetic model for growth of Au-catalyzed ZnO nanorods: theory and experiment. J. Cryst. Growth **309**(1), 70–75 (2007)

Huang, B., Zeng, W., Li, Y.: Synthesis of ZIF-8 coating on ZnO nanorods for enhanced gas-sensing performance. Chemosensors **10**(8), 297–312 (2022)

Hughes, W.L., Wang, Z.L.: Formation of piezoelectric single-crystal nanorings and nanobows. J. Am. Chem. Soc. **126**(21), 6703–6709 (2004)

Ismail, M.A., Taha, K.K., Modwi, A., Khezami, L.: ZnO nanoparticles: Surface and X-ray profile analysis. J. Ovonic Res. **14**(5), 381–393 (2018)

Kaiser, A., Ceja, E.T., Huber, F., Herr, U., Thonke, K." Highly sensitive H_2S sensing with gold and platinum surface-modified ZnO nanowire ChemFETs. In: Proceedings, p. 7. MDPI (2020)

Kar, S., Pal, B.N., Chaudhuri, S., Chakravorty, D.: One-dimensional ZnO nanostructure arrays: synthesis and characterization. J. Phys. Chem. B **110**(10), 4605–4611 (2006)

Kim, H.-M., Park, J.-H., Lee, S.-K.: Fiber optic sensor based on ZnO nanowires decorated by Au nanoparticles for improved plasmonic biosensor. Sci. Rep. **9**(1), 1–9 (2019)

Kołodziejczak-Radzimska, A., Jesionowski, T.: Zinc oxide—from synthesis to application: a review. Materials (basel) **7**(4), 2833–2881 (2014)

Kong, Y.C., Yu, D.P., Zhang, B., Fang, W., Feng, S.Q.: Ultraviolet-emitting ZnO nanowires synthesized by a physical vapor deposition approach. Appl. Phys. Lett. **78**(4), 407–409 (2001)

Kononenko, O.V., Redkin, A.N., Baranov, A.N., Panin, G.N., Kovalenko, A.A., Firsov, A.A.: ZnO nanorods: synthesis by catalyst-free CVD and thermal growth from salt composites and application to nanodevices. Nanorods Nanotechnol. Nanomater. 51–74 (2012). https://doi.org/10.5772/34936

Kumar, R.T.R., et al.: Growth of ZnO nanostructures on Au-coated Si: influence of growth temperature on growth mechanism and morphology. J. Appl. Phys. **104**(8), 84309 (2008)

Kumar, S., Sahare, P.D., Kumar, S.: Optimization of the CVD parameters for ZnO nanorods growth: its photoluminescence and field emission properties. Mater. Res. Bull. **105**, 237–245 (2018)

Kumbhakar, P., Singh, D., Tiwary, C.S., Mitra, A.K.: Chemical synthesis and visible photoluminescence emission from monodispersed ZnO nanoparticles. Chalcogenide Lett. **5**(12), 387–394 (2008)

Levitt, A.P.: VLS Growth Mechanism of Crystal Growth in Whisker Technology. Wiley-Interscience, New York (1971)

Li, Y., et al.: Au-catalyzed growth processes and luminescence properties of ZnO nanopillars on Si. J. Appl. Phys. **99**(5), 54307 (2006)

Lim, Y.S., Park, J.W., Kim, M.S., Kim, J.: Effect of carbon source on the carbothermal reduction for the fabrication of ZnO nanostructure. Appl. Surf. Sci. **253**(3), 1601–1605 (2006)

Lockett, A.M., Thomas, P.J., O'Brien, P.: Influence of seeding layers on the morphology, density, and critical dimensions of ZnO nanostructures grown by chemical bath deposition. J. Phys. Chem. C **116**(14), 8089–8094 (2012)

Malik, S., Muhammad, K., Waheed, Y.: Nanotechnology: a revolution in modern industry. Molecules **28**(2), 661–686 (2023)

Mazhdi, M., Hossein, K.P.: Structural characterization of ZnO and ZnO: Mn nanoparticles prepared by reverse micelle method Int. J. Nano Dim. **2**(4), 233–240 (2012)

Mirzaei, H., Darroudi, M.: Zinc oxide nanoparticles: biological synthesis and biomedical applications. Ceram. Int. **43**(1), 907–914 (2017)

Navas, M.P., Soni, R.K., Tarasenka, N., Tarasenko, N.: Temperature and solution assisted synthesis of anisotropic ZnO nanostructures by pulsed laser ablation. Appl. Surf. Sci. **414**, 413–423 (2017)

Patterson, A.L.: The Scherrer formula for X-ray particle size determination. Phys. Rev. **56**(10), 978–982 (1939)

Paul, D.R., Robeson, L.M.: Polymer nanotechnology: nanocomposites. Polymer (guildf) **49**(15), 3187–3204 (2008)

Purica, M., Budianu, E., Rusu, E., Danila, M., Gavrila, R.: Optical and structural investigation of ZnO thin films prepared by chemical vapor deposition (CVD). Thin Solid Films **403**, 485–488 (2002)

Rosli, N., et al.: Random lasing emission of ZnO nanorods from different seeding thickness. In: Journal of Physics: Conference Series, p. 12018. IOP Publishing (2022)

Rusli, N.I., Tanikawa, M., Mahmood, M.R., Yasui, K., Hashim, A.M.: Growth of high-density zinc oxide nanorods on porous silicon by thermal evaporation. Materials (basel) **5**(12), 2817–2832 (2012)

Saeed, N.M.: Preparation and properties of nanostructure zinc oxide thin films. Iraqi J. Phys. **7**(8), 75–81 (2009)

Sangpour, P., Roozbehi, M., Akhavan, O., Moshfegh, A.Z.: ZnO nanowires from nanopillars: influence of growth time. Curr. Nanosci. **5**(4), 479–484 (2009)

Schulz, H., Thiemann, K.H.: Structure parameters and polarity of the wurtzite type compounds Sic—2H and ZnO. Solid State Commun. **32**(9), 783–785 (1979)

Shi, J., Zhang, J., Yang, L., Qu, M., Qi, D., Zhang, K.H.L.: Wide bandgap oxide semiconductors: from materials physics to optoelectronic devices. Adv. Mater. **33**(50), 2006230 (2021)

Siegel, J., Lyutakov, O., Rybka, V., Kolská, Z., Švorčík, V.: Properties of gold nanostructures sputtered on glass. Nanoscale Res. Lett. **6**, 1–9 (2011)

Singh, A., Vishwakarma, H.L.: Study of structural, morphological, optical and electroluminescent properties of undoped ZnO nanorods grown by a simple chemical precipitation. Mater. Sci. **33**(4), 751–759 (2015)

Soleimanpour, A.M., Khare, S.V., Jayatissa, A.H.: Enhancement of hydrogen gas sensing of nanocrystalline nickel oxide by pulsed-laser irradiation. ACS Appl. Mater. Interfaces **4**(9), 4651–4657 (2012)

Song, J., Lim, S.: Effect of seed layer on the growth of ZnO nanorods. J. Phys. Chem. C **111**(2), 596–600 (2007)

Sun, Y., et al.: The applications of morphology controlled ZnO in catalysis. Catalysts **6**(12), 188 (2016)

Tseng, Y.-K., Hsu, H.-C., Hsieh, W.-F., Liu, K.-S., Chen, I.-C.: Two-step oxygen injection process for growing ZnO nanorods. J. Mater. Res. **18**(12), 2837–2844 (2003)

Wahab, R., et al.: Zinc oxide nanostructures and their applications. Intell. Nanomater. Process. Prop. Appl. **28**, 183–212 (2012)

Wang, H., et al.: Selective growth of vertical-aligned ZnO nanorod arrays on Si substrate by catalyst-free thermal evaporation. Nanoscale Res. Lett. **3**, 309–314 (2008)

Yi, G.-C., Wang, C., Park, W.I.: ZnO nanorods: synthesis, characterization and applications. Semicond. Sci. Technol. **20**(4), S22–S34 (2005)

Young, S.-J., Chu, Y.-L.: Hydrothermal synthesis and improved CH_3OH-sensing performance of ZnO nanorods with adsorbed Au NPs. IEEE Trans. Electron Devices **68**(4), 1886–1891 (2021)

Young, S.-J., Lai, L.T.: Investigation of a highly sensitive Au nanoparticle-modified ZnO nanorod humidity sensor. IEEE Trans. Electron Devices **68**(2), 775–779 (2021)

Young, S.-J., Chu, Y.-J., Chen, Y.-L.: Enhancing pH sensors performance of ZnO nanorods with Au nanoparticles adsorption. IEEE Sens. J. **21**(12), 13068–13073 (2021)

Yu, X., Marks, T.J., Facchetti, A.: Metal oxides for optoelectronic applications. Nat. Mater. **15**(4), 383–396 (2016)

Zak, A.K., Majid, W.H.A., Abrishami, M.E., Yousefi, R.: X-ray analysis of ZnO nanoparticles by Williamson-hall and size–strain plot methods. Solid State Sci. **13**(1), 251–256 (2011)